Integrated Analysis of Tumor-Associated Macrophage Infiltration and Prognosis in Ovarian Cancer

qianxia tan
Xiangya Hospital Central South University
huining liu
Xiangya Hospital Central South University
jie xu
Xiangya Hospital Central South University
yanqun mo
Xiangya Hospital Central South University
chenchun wu
Xiangya Hospital Central South University
furong dai (murmansk2020@csu.edu.cn)
Xiangya Hospital Central South University https://orcid.org/0000-0002-1903-0010

Primary research

Keywords: Ovarian cancer, tumor immune infiltration, tumor-associated macrophage, WGCNA, prognosis,

Posted Date: June 23rd, 2021

DOI: https://doi.org/10.21203/rs.3.rs-635651/v1

Abstract

Background

Most ovarian cancer patients with poor prognosis and immune microenvironment play a vital role in the progression of ovarian cancer. We aim to develop a tumor-associated macrophage related gene (TAMRGs) prognostic signature that can stratify and predict overall survival for ovarian cancer.

Methods

We acquired single cell and bulk transcriptome raw data of ovarian cancer from The Cancer Genome Atlas (TCGA) and Gene Expression Omnibus (GEO). The immune landscape was identified in primary and ascites of ovarian cancer. CIBERSORT deconvolution algorithm, Weighted gene co-expression network analysis (WGCNA), univariate cox analysis, LASSO algorithm, and multivariate cox analysis were performed for the identification of TAMRG and the development of prognostic signature.

Results

We identified inter-and intra-patient heterogeneity for immune infiltration cells at a single-cell resolution. Tumor infiltration macrophages showed immunosuppressive characteristics with an M2 phenotype. T cell CD4 memory activated, mast cell activated, neutrophils and macrophages M2 were negatively correlated with overall survival, while macrophages M1 was positively correlated. A total of 219 TAMRGs were identified and a novel 6-gene signature (TAP1, CD163, VSIG4, IGKV4-1, CD3E, and MS4A7) with superior prognostic independence was established.

Conclusions

The TAMRG-based signature is expected to be a promising target for prognosis and treatment response of ovarian cancer.

Background

Ovarian cancer (OC), accounts for the highest mortality rate among gynecological malignancies, with 13770 estimated new deaths in the United States, 2021(1). More than 70% of cases of OC are diagnosed at advanced stages with five-year survival rates approximating 48%(2). Despite appropriate surgery and platinum-based chemotherapy, most patients with ovarian cancer relapse and disseminates(3). It is urgent to identify novel clinical biomarkers and develop new therapeutic strategies for ovarian cancer.

Recent evidence has unraveled the tumor microenvironment (TME) plays a vital role in the metastasis of ovarian cancer and is considered a possible therapeutic target for ovarian cancer(4). Among solid tumors, TME of epithelial ovarian cancer is unique because the cancer cells are frequently shed from the primary tumor into the peritoneal cavity, build up a sole microenvironment of malignant ascites. The treatment of ovarian cancer targeting the tumor microenvironment is developing rapidly. Targets mainly focusing on

angiogenesis, tumor-associated macrophages, cancer-associated fibroblasts, and immune checkpoint blockade(5, 6).

Ovarian cancer is a kind of highly heterogenous tumor; the diversified TME of ovarian cancer is one manifestation of this fact. Jiménez-Sánchez et al reported that different metastases exhibited concomitant regression and progression in a high-grade serous ovarian cancer (HGSOC) patient who received multiple times of chemotherapy. Tumor progression/regression is associated with immune cell infiltration and specific subsets oligoclonal expansion of T cells (7). Their further study found that inflammatory microenvironment and immune-cell-excluded coexist in the same individual and tumor site in untreated HGSOC, indicating ubiquitous variation in immune cell infiltration (8). Therefore, identifying the subset of highly metastatic tumor cells and the diversity of OC cells at single-cell level might contribute to the precision treatment of OC.

As an important part of the TME, immune cells include lymphocytes, macrophages, mast cells, neutrophils, dendritic cells (DCs), myeloid-derived suppressor cells (MDSCs)(9). Tumor-associated macrophages (TAM) are the most frequently found of immune cells that participate in inflammation and tumorigenesis present in the ovarian TME(10). TAM mainly promotes tumor growth and is at the center of the invasion and metastasis microenvironment(11). Clinical studies indicated that a high abundance of TAMs is associated with poor prognosis(12). Macrophages can be classified into M1 and M2 types(13). Most TAMs are considered to have an M2 phenotype while promoting tumor angiogenesis and tissue remodeling. M1 and M2 macrophages are plastic and their phenotype is defined by their gene expression profile rather than by deterministic differentiation pathways and lineage choices.

In this study, we integrated scRNA-seq and bulk RNA-seq to develop and validate a TAM-based prognostic signature for ovarian cancer. First, we identified TME of the high-grade serous ovarian cancer ascites samples using seRNA-seq data. Second, we explored the function status of immune cells and found that M2-like tumor-associated macrophages were enriched. Third, we estimated TAM related genes using bulk RNA-seq data. Then, TAP1, CD163, VSIG4, IGKV4-1, CD3E, and MS4A7 were identified as the 6 key OS-predicting gene signatures. Finally, the prognostic module was validated using the validation set from the GEO. Identifying prognostic markers of ovarian cancer based on a large-scale public cohort of gene expression data may provide new therapeutic targets for more efficacious treatment of OC.

Methods

Data acquisition and preprocessing

The scRNA-seq data and bulk RNA-seq data of human ovarian cancer samples were included in this study for analysis. The scRNA-seq data of a total of 9609 cells of 6 human high grade serous ovarian cancer (HGSOC) ascites samples, accession number GSE146026, were obtained from the Gene Expression Omnibus (GEO, http://www.ncbi.nlm.nih.gov/geo/) database, with a reading depth of 10X genomics based on Illumina NextSeq 500. The bulk RNA-seq profiles of ovarian cancer samples were obtained from the TCGA database (https://portal.gdc.cancer.gov/) and the GEO database. We excluded

samples with unavailable clinical information and ultimately included 375 ovarian cancer samples from the TCGA cohort as the training set and 185 ovarian cancer samples from the GEO cohort (GSE26712) as the validation set.

Single cell RNA-seq analysis

R4.0.5 was used to perform all the analyses. The Seurat 3.0 package was used for quality control, statistical analysis, and exploration of the scRNA-seq data(14). First, genes detected in < 3 cells, cells with < 200 total detected genes, and pre-mito ≥ 5% were used as quality control standards. In total, 9609 cells were included in this analysis. Then, the gene expression was normalized using a linear regression model. PCA was performed to identify significantly available dimensions with a P value < 0.05. Then, the t-distributed stochastic neighbor embedding (tSNE) algorithm was applied for dimensionality reduction with 20 initial PCs and for performing cluster classification analysis across all cells. The differential expression analysis among all genes within cell clusters was performed using the Wilcox to identify the marker genes of each cluster. |log2[fold change (FC)]| > 0.5 and P value < 0.05 were considered the cutoff criteria for identifying marker genes. Afterward, cell cluster biomarkers were found and annotated by the singleR package.

Gene Set Variation Analysis of immune cells

Gene Set Variation Analysis (GSVA), a gene set enrichment method that estimates variation of pathway activity over a sample population in an unsupervised manner(15). The enrichment scores of the gene sets were evaluated using GSVA package in R. The immune cells related gene sets were obtained from MSigDB and supplementary files provided by Woosung Chung et al(16).

Estimate of the abundance of tumor immune infiltration and survival analysis

CIBERSORT R script was performed to estimate the abundance of 22 tumor immune infiltration cell types in TCGA OV based on the bulk RNA-seq dataset(17). According to the median of each immune cell enrichment score, the samples were divided into two groups to compare the overall survival. R package “survival” and “survminer” were used to perform Survival analysis.

Construction of weighted correlation network analysis (WGCNA)

WGCNA was performed with the R package “WGCNA”(18). A power of β = 3 and a scale-free R^2>0.85 were set as soft-threshold parameters to ensure a signed scale-free co-expression gene network. We used the dynamic hybrid cutting method to classify genes with similar expression patterns, the minimum size cut-off of the module is 30. Module eigengenes were used to execute the component analysis of each module. We estimated the correlation between tumor immune infiltration enrichment score and module eigengenes to determine the significance of modules by Pearson test. The interested macrophages subtypes and modules were selected for follow-up analysis. The key genes were identified by gene

significance (GS) and module membership (MM). The genes in the module with |GS|>0.2 and MM>0.8 were considered to be significant.

Identification of molecular subtype

"ConsensusClusterPlus" package in R was utilized to perform K-means-based unsupervised consensus clustering based on the expression patterns of the TAM-related gene signature(19). Cumulative distribution function (CDF) plots and consensus matrices were obtained with 1000 iterations, 80% resampling rate Pearson correlation. Then, we compared overall survival between different clusters using Kaplan-Meier survival analysis. Gene set enrichment analysis (GSEA) was performed to explore potential molecular mechanisms. We also performed comparisons of 6 immune checkpoints (PDCD1, CTLA4, CD274, CD80, PDCD1LG2, CD86) between different clusters.

Establishment and estimation of the prognostic risk score model

First, univariate Cox regression analysis was used to evaluate the associations between TAM-related genes and survival in TCGA training set. Second, Least Absolute Shrinkage and Selection Operator (LASSO) and multivariate Cox regression analyses were applied to identify the prognosis-related genes with a P value < 0.05. Subsequently, a risk score model based on the key prognosis-related TAMRG-based gene was established to predict the prognosis of OV patients. We calculated the risk score by a linear method to assemble the coefficient and expression level of the prognostic gene. The formula as follows: Risk score = Expgene1 × β1 + Expgene2 × β2 +…+ Expgenen × βn, in which "Exp" represents the expression level of the prognostic genes, and "β" represents the regression coefficient.

Accordingly, the patients in TCGA training set were divided into the low-risk group or the high-risk group based on the median risk score. Kaplan-Meier survival analysis was used to compare the OS of these two groups. Time-dependent ROC curve analysis and Harrell's concordance index (C-index) were utilized by the "survivalROC" and "survminer" packages in R to evaluate the prediction accuracy of the risk score prognostic model. Finally, the prognostic model generated by the TCGA training cohort was verified in the GEO validation cohort. We also performed a comparison of the C-index between the prognostic model and age, stage, grade, debulking, and 9 published signatures.

Statistical analyses

T test was used to compare the mean values between the two groups. In the survival analysis, associations between characteristics and overall survival were evaluated by Cox proportional hazard models. Kaplan-Meier survival curves were drawn and compared among subgroups using log-rank tests. The C-index and receiver operating characteristic (ROC) curve were estimated using R package survival, survminer, and survivalROC.

Statistical analyses were performed using R version 4.0.5 (The R Foundation). P values were two-sided, and $P < 0.05$ was considered statistically significant.

Results

Tumor cell heterogeneity in ovarian cancer

A schematic diagram of the study design was shown in Figure 1. Following the quality control standard, 9609 cells from ascites samples of ovarian cancer patients were included in the analysis (Figure 2A and B). Variance analysis showed 1500 highly variable genes in a total of 10048 corresponding genes, and the top 10 are IGLL5, IGJ, WT1-AS, CCL17, GNLY, CCL5, MZB1, HBB, and NKG7 (Figure 2C). Principal component analysis (PCA) was performed to identify available dimensions and screen correlated genes. PCA showed a mixed representation of cells intra-and inter-patient (Figure 2D). PCA results revealed that the P value of the first 20 principal components (PCs) were less than 0.05, we selected 20 PCs for follow-up analysis (Figure 2E). Afterward, ovarian cancer cells were successfully classified into 13 separate clusters by the t-distributed stochastic neighbor embedding (tSNE) algorithm (Figure 2F). A total of 6453 marker genes were identified and the top 10 differential expression genes from all 13 clusters were displayed in the heatmap (Figure 2G).

Identification of immune cells and GSVA

The resulting cell clusters were annotated as epithelial, stromal (fibroblasts, endothelial cells, and melanocytes), or immune cells (Figure 3A) by singleR and established marker genes(20). Cluster 9 and 10 containing 419 cells, was annotated as epithelial cells; clusters 2 and 7, containing 1895 cells, were annotated as stromal cells; cluster 0, 1, 3, 4, 5, 6, 7, 8, 11 and 12, containing 6706 cells, was annotated as immune cells. Immune cells (n =6706) were subsetted and annotated as macrophages, B cells, T cells, and Dendritic cells (DC); cluster0, 1, 3, and 4, containing 5930 cells, were annotated as macrophages; clusters 6, containing 384 cells, was annotated as B cells; cluster 8, containing 320 cells, was annotated as T cells; cluster 12, containing 72 cells, was annotated as DC (Figure 3B).

GSVA has been performed to analyze the B cell function status, such as anti-apoptosis, pro-apoptosis, proliferation, Naïve, cytokines, and Germinal center. The function status of pro-apoptosis showed heterogeneity in the same patient (Supplement figure1). For T cells, we estimated cytotoxic, native, regulatory, exhausted, costimulatory, G1/S, and G2/M related gene signatures. The function status of cytotoxic in patient2 is significantly enriched (Supplement figure2). Figure 3C showed a comprehensive analysis of the four kinds of immune cells. Macrophages are the largest proportion (88.4%) of immune cells. M2 up signature was highly enriched in macrophages (Figure 3C). Macrophages marked by CD163, CSF1R, MS4A7, VSIG4; B cells marked by CD79B, MZB1; T cells marked by CD2, CD3D; DC marked by CD1E, CD83 (Figure 3D). In summary, B cells, T cells, and macrophages showed heterogeneity in the same patient and among different patients.

High M2 and low M1 were associated with poor survival in ovarian cancer patients

CIBERSORT based Nu support vector regression algorithm was performed to calculate the immune score of the transcribed profile of bulk RNA seq data from TCGA-OV patients. The estimated proportion of 22

immune cell types was shown in Figure 4A and 4B. Among them, four kinds of tumor immune infiltration cells were negatively correlated with overall survival of OV patients, including macrophages M2 (P=0.031), mast cell activated (P=0.0033), T cell CD4 memory activated (P=0.04), and neutrophils (P=0.027), while macrophages M1 (P=0.00042) were positively correlated with overall survival of OV patients.

Identification of TAM-related genes

The expression values of 4043 genes with a coefficient of variation values greater than 0.1 were utilized to construct the gene co-expression network of OV by R package WGCNA. The samples of TCGA-OV were clustered by the average linkage and Pearson's correlation values. We selected β = 3 (scale free R^2 > 0.9) as the soft-thresholding power to construct a scale-free network. Dynamic hybrid cutting was used to construct a hierarchical clustering tree. Each tree leaf represented a single gene on the tree. A series of genes with similar expression data are clustered into branches to form a gene module. Furthermore, 10 modules were constructed (Figure 5A). Among 10 modules, the turquoise module had a strong relationship with the black and pink module (Figure 5B).

We correlated gene module and CIBERSORT fraction, found that the black module showed a higher correlation with macrophage M1(R^2=0.52, P=2e-27) and B cell naïve (R^2=0.5, P=5e-25), the pink module was highly correlated to macrophage M1 (R^2=0.54, P=2e-30) and T cell CD8 (R^2=0.36, P=1e-12), and the turquoise module was highly correlated to macrophage M1 (R^2=0.47, P=1e-22) and macrophage M2 (R^2=0.31, P=1e-09; Figure 5C). We were interested specifically in macrophages, so focused on the black, pink, and turquoise module that showed correlation with macrophages was identified as TAM-related modules. The scatter diagram showed a highly positive correlation between gene significance and module membership in the black module (cor=0.9, P=4.9e-32), turquoise module (cor=0.73, P=8.9e-124), and pink module (cor=0.79, P=3.6e-17; Figure 5D), indicating that these modules are highly correlated with TAMs. According to the cut-off criteria, 219 genes in 3 modules were identified as TAM-related gene signatures (Supplement table1).

Molecular subtype based on TAM-related gene signature

To establish a classification of the expression patterns of the 219 TAM-related gene signatures, K-means-based unsupervised consensus clustering was performed on 375 OV patients from the TCGA database. The cumulative distribution function (CDF) plot showed k =2 (from 2 to 6) is the optimal number of clusters (Figure 6A). The consensus heatmap showed all OV patients were classified into two clusters: 151 (40.0%) in cluster 1 and 224 (60.0%) in cluster 2 (Figure 6B). The heatmap revealed the differentially expressed genes between the two molecular subtypes (Figure 6C). Kaplan- Meier survival analysis indicated that patients with cluster 1 had a significantly better OS than patients with cluster 2 (P=0.0071) (Figure 6D). The violin plot showed that cluster 1 had significantly higher macrophages M1 scores compared to cluster 2 (P=6.8e-13; Figure 6E). GSEA was performed on cluster one over cluster two of OV patients. Upregulated pathways included pathways related to apoptosis, antigen processing and

presentation, angiogenesis, epithelial mesenchymal transition (EMT), and macrophage M1 upregulation in cluster one (Figure 6F). We compared 6 main immune checkpoints between two molecule subtypes of OV patients. PDCD1 (PD1; P=6.2e-10), CTLA4(P=6.6e-16), CD274 (PDL1; P=5.4e-06), CD80(P=7.7e-07), PDCD1LG2 (PDL2; P=1.9e-10), and CD86 (P=1.6e-05) were highly expressed in Cluster 1 (Figure 6G).

CD163, TAP1, VSIG4, MS4A7, CD3E, and IGKV4-1 are the 6 most significant survival-predicting TAMRG-based signature in human OV

Univariate Cox analysis was performed, and 25 prognosis-associated TAM-based signatures were identified in the TCGA training set (Supplement figure 3A). Least absolute shrinkage and selection operator (LASSO) followed by multivariate Cox analysis was then performed, and 6 significant survival-predicting GDRGs were identified (Supplementary Figure 3B and 3C): CD163 (HR=1.19, 95%CI 1.05-1.34, P<0.01), transporter 1 (TAP1, HR=0.74, 95%CI 0.63-0.87, P<0.001), V-set and immunoglobulin domain containing 4 (VSIG4, HR=1.15, 95%CI 1.04-1.28, P<0.01), immunoglobulin kappa chain variable 4-1 (IGKV4-1, HR=0.64, 95%CI 0.47-0.86, P<0.01), CD3E (HR=0.82, 95%CI 0.70-0.96,, P=0.016), and membrane spanning 4-domains A7 (MS4A7, HR=1.16, 95%CI 1.02-1.32, P=0.023). We explored the expression of 6 gene signatures in the scRNA-seq set (Supplement figure 4A; MS4A7, VSIG4, and IGKV4-1 were not provided). CD163, MS4A7, and VSIG4 were significantly upregulated in macrophages. CD3E was significantly upregulated in T cells. TAP1 was upregulated in macrophages and B cells. The expression of IGKV4-1 was not detected. Furthermore, Gene Expression Profiling Interactive Analysis (GEPIA) database was performed to explore the expression of these 6 gene signatures in 426 OV (TCGA) samples and 88 normal (GTEx) samples. We found that CD163 was upregulated, while TAP1, CD3E, and IGKV4-1 were downregulated in OV compared to normal samples (Supplementary Figure 4B).

Generation and validation of the 6 gene signatures based prognostic risk score model

The prognostic risk score model was developed based on the above 6 gene signatures with the following formula: Risk score = ExpCD163 ´ 0.0284 + ExpCD3E ´ (-0.0297) + ExpIGKV4 ´ (-0.0007) + ExpTAP1 ´ (-0.0130) + ExpVSIG4 ´ 0.0009 + ExpMS4A7 ´ 0.0487. The risk scores of all patients in the TCGA training set were calculated, and the patients were divided into either a high-risk (high score) group or a low-risk (low score) group using the median value of the risk score as the cutoff value (Figure 7B). Kaplan-Meier survival analysis demonstrated that patients in the high-risk group had significantly poorer OS than those in the low-risk group (log-rank, P = 0.00016; Figure 7A). The C-index of the 6 gene signature for OS prediction was 0.614 (95% CI=0.593 to 0.636). Time-dependent receiver operating characteristic (ROC) analysis also indicated that the 6 gene signature showed excellent performance in predicting the 3-, 5- and 10-year OS rates, with respective area under the curve (AUC) values of 0.624, 0.68, and 0.718 (Figure 7C). The relationship between infiltration proportion of six immune cell types and the risk score was analyzed to validate the effect of 6 gene signatures on TAM-related genes. A significantly negative correlation was found between the risk score and infiltration proportion of the macrophages M1 (R=0.38, P=1.4e-14). The infiltration proportion of macrophages M2 was positively correlated with the risk score (R=0.29, P=1.3e-08; Supplement figure 4C).

Then, the predictive formula was validated similarly using the GEO cohort. As shown in Figure 7E, 185 OV patients were classified into high-risk or low-risk groups. Consistent with the results from the TCGA training set, the survival analysis also demonstrated that patients in the high-risk group had significantly poorer OS than patients in the low-risk group (log-rank, P = 0.0026; Figure 7D). The C-index of the 6 gene signature was 0.611 (95% CI=0.584 to 0.638). Time-dependent ROC analysis also suggested favorable values in predicting the 3-, and 5-year OS rates, with a respective area under the curve (AUC) values of 0.674, and 0.704 in the GEO validation set (Figure 7E). These results indicate that the TAM-based prognostic risk score model can serve as a prognostic predictor for different populations of OV patients.

Comparison with clinical characteristics and other signatures

We compared the model predictive accuracy of 6 gene signatures with clinical characteristics including age, stage, grade, and residual as well as 8 reported ovarian cancer prognostic signatures. Continuous prognostic scores were calculated from each signature to compare among different datasets. Of the 13 survival predicted factors, MPSOV had a highest mean C-index (0.613) compared with stage (0.519), grade (0.532), age (0.593), residual (0.556; Supplement table 2) and other signatures (0.516 to 0.584; Supplement table 3).

Discussion

In solid tumors, malignant cells and many other types of non-malignant cells form a unique microenvironment that can modify the tumor characteristics of tumor cells(12). We analyzed tumor heterogeneity for tumor immune infiltration cells using scRNA-seq and bulk RNA-seq set. At a single-cell level, most of the non-malignant cells were identified as immune cells, with four distinct clusters of B cells, T cells, DCs, and macrophages. Inter- and intra-patient heterogeneity was observed for tumor infiltration immune cells in HGSOC. Both macrophages and T cells showed immunosuppressive characteristics: macrophages with an M2 phenotype and T cells with an exhausted phenotype. The existence of M2 TAMs in tumor tissues is an important contributing factor for the formation of the immunosuppressive TME(21). M2 macrophages express the ligand receptors for CTLA-4 and PD-1. The activation of PD-1 and CTLA-4 inhibits cytotoxic function and regulates the cell cycle of T cells(22). These findings suggested that an important reason for the wide tumor heterogeneity of ovarian cancer transcriptome is distinct immune system status and dynamic immune cell interactions in the surrounding microenvironment.

CIBERSORT was performed to estimate tumor infiltration immune cells at bulk RNA-seq resolution, and its correlation with prognosis was analyzed. T cell CD4 memory activated, mast cell activated, neutrophils and macrophages M2 were negatively correlated with overall survival of OC patients, while macrophages M1 infiltration indicated better clinical outcomes. Similarly, CD4 + CD25 + FOXP3 + Treg cells infiltration was associated with reduced survival and high death hazard in 104 individuals affected with ovarian cancer(23). Several studies revealed the increased density of M2-like TAMs was associated with poor OS (24–26). However, the relationship between M2 density and OS is controversial in OC. Zhang et al(27)

reported no significant correlation between these two factors, while Lan et al(28) found a negative correlation consistent with our results. This may be due to different types of tumor tissue.

219 TAM-related gene signatures (TAMRGs) were established by WGCNA. The patients with OC were classified into two groups by unsupervised clustering method to evaluate the prognostic value of TAM related gene signature. Cluster 1 with a high infiltration of macrophage M1(M1 like TAM) was associated with a better prognosis, indicating that the TAMRG-based patient classification can be used to predict patient survival. GSEA showed that M1like TAM not only enriched in immune-related pathways, but also enriched in angiogenesis, EMT, and JAK-STAT3. However, macrophages M2 are the main TAM in ovarian cancer and are associated with tumor angiogenesis, invasion, metastasis, and early recurrence(12, 29, 30). The simple dichotomy of M1/M2 macrophages may not explain the complexity of TAM heterogeneity(31). M1 and M2 macrophages can be considered as two extremes of a continuum of functional states(31, 32), the sub-populations of TAMs in between the two extremes can share characteristics of both M1 and M2 types(33). For example, a recent study revealed that TAMs could co-express M1/M2 markers, together with T cell co-inhibitory and co-stimulatory receptors(34). In addition, Müller S identified phenotypic differences in TAMs of distinct lineages at single cell resolution in human gliomas. The results indicated that TAMs frequently co-express M1 and M2 type genes in individual cells which increased the difficulty of isolating them(35). TAMs are plastic, and their functional phenotypes and distribution show reversible changes in response to different microenvironment stimuli(31, 36–38). In summary, these findings may provide evidence to the existence of the intermediate state of TAMs.

Immunotherapy can alleviate the immunosuppression status in the tumor, which is a promising treatment strategy. It has been reported that it can significantly prolonged progression-free survival and overall survival of patients with melanoma(39) and non-small-cell lung cancer(40). Unfortunately, although numerous trials have been conducted, the outcomes of trials including immune check-point inhibitors in OC either when used as single agents or in combination with antiangiogenic therapy have not been as effective as expected. Our results revealed that cluster 1 with increased macrophage M1 density expressed more PD1/PDL1/PDL2, and CTLA4/CD80/CD86 molecules. Based on these findings, we speculated that cluster 1 with increased macrophage M1 density may benefit more from anti-PD1 and anti-CTLA4 therapies.

In the present study, CD163, TAP1, VSIG4, MS4A7, CD3E, and IGKV4-1were identified as the 6 most significant survival-predicting TAMRG in OC. A risk score module was successfully established based on these TAMRG and then validated in the GEO set. As far as we know, this prognostic module is the first to incorporate a TAM-related signature for predicting OC patient survival. Although the absolute value of prognostic module C- index is not very high, it is superior to the traditional clinical factors and has a significant improvement in the comprehensive model. Therefore, this module can be used better to estimate the prognosis of patients and classify them into different subgroups to benefit from different treatments.

We acknowledged some limitations in the present research. We downloaded data from the published database (TCGA and GEO). Some patients' details are incomplete, such as grade, medical history, e.g., not available for multivariate cox analysis. This study is a retrospective study, so further prospective large-scale trials are needed to verify the clinical application value.

Conclusions

In the current study, We constructed a novel 6 gene signatures associated with the prognosis of OC patients based on TAMRG. The TAMRG-based signature is expected to be a promising target for prognosis and treatment response of ovarian cancer.

Declarations

Ethics approval and consent to participate

Not applicable.

Consent for publication

Not applicable.

Availability of data and materials

The public datasets used in our study can be found on https://portal.gdc.cancer.gov/ and https://www.ncbi.nlm.nih.gov/.

Competing interests

No potential conflict of interest.

Funding

This research was supported by the Nature Scientific Foundation of China (grant number: 81472434).

Authors' contributions

QT and FD initiated the comprehensive study, QT, HL and FD wrote the main manuscript text, JX, YM and CW analyzed the data and prepared all figures. All authors reviewed the manuscript.

Acknowledgements

The data of this study is obtained by the TCGA database and GEO database. We are grateful to them for providing data sources for our research.

References

1. Siegel RL, Miller KD, Fuchs HE, Jemal A. Cancer Statistics. 2021. *CA: a cancer journal for clinicians*. (2021)71(1):7–33 doi:10.3322/caac.21654.
2. Kuroki L, Guntupalli SR. Treatment of epithelial ovarian cancer. BMJ (Clinical research ed. 2020;371:m3773. doi:10.1136/bmj.m3773.
3. Bowtell DD, Böhm S, Ahmed AA, Aspuria PJ, Bast RC Jr, Beral V, et al. Rethinking ovarian cancer II: reducing mortality from high-grade serous ovarian cancer. Nature reviews Cancer. 2015;15(11):668–79. doi:10.1038/nrc4019.
4. Luo Z, Wang Q, Lau WB, Lau B, Xu L, Zhao L, et al. Tumor microenvironment: The culprit for ovarian cancer metastasis? Cancer letters. 2016;377(2):174–82. doi:10.1016/j.canlet.2016.04.038.
5. Jiang Y, Wang C, Zhou S. Targeting tumor microenvironment in ovarian cancer: Premise and promise. Biochimica et biophysica acta Reviews on cancer. 2020;1873(2):188361. doi:10.1016/j.bbcan.2020.188361.
6. Yang Y, Yang Y, Yang J, Zhao X, Wei X. Tumor Microenvironment in Ovarian Cancer: Function and Therapeutic Strategy. Frontiers in cell developmental biology. 2020;8:758. doi:10.3389/fcell.2020.00758.
7. Jiménez-Sánchez A, Memon D, Pourpe S, Veeraraghavan H, Li Y, Vargas HA, et al. Heterogeneous Tumor-Immune Microenvironments among Differentially Growing Metastases in an Ovarian Cancer Patient. Cell. 2017;170(5):927 – 38.e20. doi:10.1016/j.cell.2017.07.025.
8. Jiménez-Sánchez A, Cybulska P, Mager KL, Koplev S, Cast O, Couturier DL, et al. Unraveling tumor-immune heterogeneity in advanced ovarian cancer uncovers immunogenic effect of chemotherapy. Nat Genet. 2020;52(6):582–93. doi:10.1038/s41588-020-0630-5.
9. Hanahan D, Weinberg RA. Hallmarks of cancer: the next generation. Cell. 2011;144(5):646–74. doi:10.1016/j.cell.2011.02.013.
10. Nowak M, Klink M. The Role of Tumor-Associated Macrophages in the Progression and Chemoresistance of Ovarian Cancer. Cells (2020)9(5) doi:10.3390/cells9051299.
11. Condeelis J, Pollard JW. Macrophages: obligate partners for tumor cell migration, invasion, and metastasis. Cell. 2006;124(2):263–6. doi:10.1016/j.cell.2006.01.007.
12. Pollard JW. Tumour-educated macrophages promote tumour progression and metastasis. Nature reviews Cancer. 2004;4(1):71–8. doi:10.1038/nrc1256.
13. Sica A, Allavena P, Mantovani A. Cancer related inflammation: the macrophage connection. Cancer letters. 2008;267(2):204–15. doi:10.1016/j.canlet.2008.03.028.
14. Butler A, Hoffman P, Smibert P, Papalexi E, Satija R. Integrating single-cell transcriptomic data across different conditions, technologies, and species. Nature biotechnology. 2018;36(5):411–20. doi:10.1038/nbt.4096.
15. Hänzelmann S, Castelo R, Guinney J. GSVA: gene set variation analysis for microarray and RNA-seq data. BMC Bioinform. 2013;14:7. doi:10.1186/1471-2105-14-7.

16. Chung W, Eum HH, Lee HO, Lee KM, Lee HB, Kim KT, et al. Single-cell RNA-seq enables comprehensive tumour and immune cell profiling in primary breast cancer. Nature communications. 2017;8:15081. doi:10.1038/ncomms15081.
17. Newman AM, Liu CL, Green MR, Gentles AJ, Feng W, Xu Y, et al. Robust enumeration of cell subsets from tissue expression profiles. Nature methods. 2015;12(5):453–7. doi:10.1038/nmeth.3337.
18. Langfelder P, Horvath S. WGCNA: an R package for weighted correlation network analysis. BMC Bioinform. 2008;9:559. doi:10.1186/1471-2105-9-559.
19. Wilkerson MD, Hayes DN. ConsensusClusterPlus: a class discovery tool with confidence assessments and item tracking. Bioinformatics. 2010;26(12):1572–3. doi:10.1093/bioinformatics/btq170.
20. Maynard A, McCoach CE, Rotow JK, Harris L, Haderk F, Kerr DL, et al. Therapy-Induced Evolution of Human Lung Cancer Revealed by Single-Cell RNA Sequencing. Cell. 2020;182(5):1232–51.e22. doi:10.1016/j.cell.2020.07.017.
21. Yang Q, Guo N, Zhou Y, Chen J, Wei Q, Han M. The role of tumor-associated macrophages (TAMs) in tumor progression and relevant advance in targeted therapy. Acta pharmaceutica Sinica B. 2020;10(11):2156–70. doi:10.1016/j.apsb.2020.04.004.
22. Noy R, Pollard JW. Tumor-associated macrophages: from mechanisms to therapy. Immunity. 2014;41(1):49–61. doi:10.1016/j.immuni.2014.06.010.
23. Curiel TJ, Coukos G, Zou L, Alvarez X, Cheng P, Mottram P, et al. Specific recruitment of regulatory T cells in ovarian carcinoma fosters immune privilege and predicts reduced survival. Nature medicine. 2004;10(9):942–9. doi:10.1038/nm1093.
24. Väyrynen JP, Haruki K, Lau MC, Väyrynen SA, Zhong R, Dias Costa A, et al. The Prognostic Role of Macrophage Polarization in the Colorectal Cancer Microenvironment. Cancer immunology research. 2021;9(1):8–19. doi:10.1158/2326-6066.cir-20-0527.
25. Cersosimo F, Lonardi S, Bernardini G, Telfer B, Mandelli GE, Santucci A, et al. Tumor-Associated Macrophages in Osteosarcoma: From Mechanisms to Therapy. Int J Mol Sci. (2020)21(15) doi:10.3390/ijms21155207.
26. Zheng X, Weigert A, Reu S, Guenther S, Mansouri S, Bassaly B, et al. Spatial Density and Distribution of Tumor-Associated Macrophages Predict Survival in Non-Small Cell Lung Carcinoma. Cancer research. 2020;80(20):4414–25. doi:10.1158/0008-5472.can-20-0069.
27. Zhang M, He Y, Sun X, Li Q, Wang W, Zhao A, et al. A high M1/M2 ratio of tumor-associated macrophages is associated with extended survival in ovarian cancer patients. Journal of ovarian research. 2014;7:19. doi:10.1186/1757-2215-7-19.
28. Lan C, Huang X, Lin S, Huang H, Cai Q, Wan T, et al. Expression of M2-polarized macrophages is associated with poor prognosis for advanced epithelial ovarian cancer. Technology in cancer research treatment. 2013;12(3):259–67. doi:10.7785/tcrt.2012.500312.
29. Reinartz S, Schumann T, Finkernagel F, Wortmann A, Jansen JM, Meissner W, et al. Mixed-polarization phenotype of ascites-associated macrophages in human ovarian carcinoma: correlation

of CD163 expression, cytokine levels and early relapse. International journal of cancer. 2014;134(1):32–42. doi:10.1002/ijc.28335.

30. Yin M, Li X, Tan S, Zhou HJ, Ji W, Bellone S, et al. Tumor-associated macrophages drive spheroid formation during early transcoelomic metastasis of ovarian cancer. J Clin Investig. 2016;126(11):4157–73. doi:10.1172/jci87252.
31. Ostuni R, Kratochvill F, Murray PJ, Natoli G. Macrophages and cancer: from mechanisms to therapeutic implications. Trends Immunol. 2015;36(4):229–39. doi:10.1016/j.it.2015.02.004.
32. Mantovani A, Sozzani S, Locati M, Allavena P, Sica A. Macrophage polarization: tumor-associated macrophages as a paradigm for polarized M2 mononuclear phagocytes. Trends Immunol. 2002;23(11):549–55. doi:10.1016/s1471-4906(02)02302-5.
33. Qian BZ, Pollard JW. Macrophage diversity enhances tumor progression and metastasis. Cell. 2010;141(1):39–51. doi:10.1016/j.cell.2010.03.014.
34. Singhal S, Stadanlick J, Annunziata MJ, Rao AS, Bhojnagarwala PS, O'Brien S, et al. Human tumor-associated monocytes/macrophages and their regulation of T cell responses in early-stage lung cancer. Science translational medicine. (2019)11(479) doi:10.1126/scitranslmed.aat1500.
35. Müller S, Kohanbash G, Liu SJ, Alvarado B, Carrera D, Bhaduri A, et al. Single-cell profiling of human gliomas reveals macrophage ontogeny as a basis for regional differences in macrophage activation in the tumor microenvironment. Genome biology. 2017;18(1):234. doi:10.1186/s13059-017-1362-4.
36. Stout RD, Jiang C, Matta B, Tietzel I, Watkins SK, Suttles J. Macrophages sequentially change their functional phenotype in response to changes in microenvironmental influences. *Journal of immunology (Baltimore, Md*: 1950). (2005)175(1):342-9 doi:10.4049/jimmunol.175.1.342.
37. Okabe Y, Medzhitov R. Tissue-specific signals control reversible program of localization and functional polarization of macrophages. Cell. 2014;157(4):832–44. doi:10.1016/j.cell.2014.04.016.
38. Kim J, Bae JS. Tumor-Associated Macrophages and Neutrophils in Tumor Microenvironment. Mediat Inflamm. 2016;2016:6058147. doi:10.1155/2016/6058147.
39. Robert C, Schachter J, Long GV, Arance A, Grob JJ, Mortier L, et al. Pembrolizumab versus Ipilimumab in Advanced Melanoma. N Engl J Med. 2015;372(26):2521–32. doi:10.1056/NEJMoa1503093.
40. Reck M, Rodríguez-Abreu D, Robinson AG, Hui R, Csőszi T, Fülöp A, et al. Pembrolizumab versus Chemotherapy for PD-L1-Positive Non-Small-Cell Lung Cancer. N Engl J Med. 2016;375(19):1823–33. doi:10.1056/NEJMoa1606774.

Figures

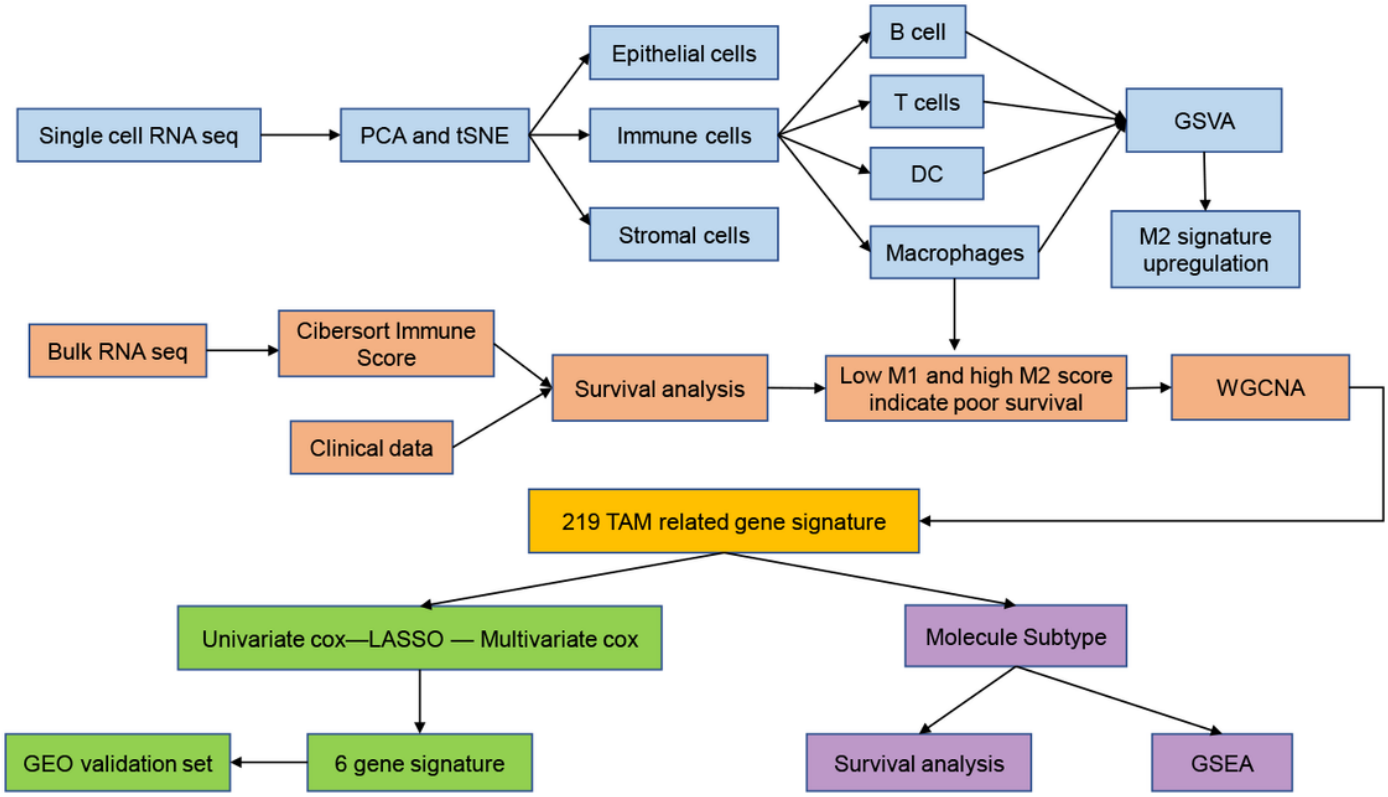

Figure 1

Schematic diagram of the study design.

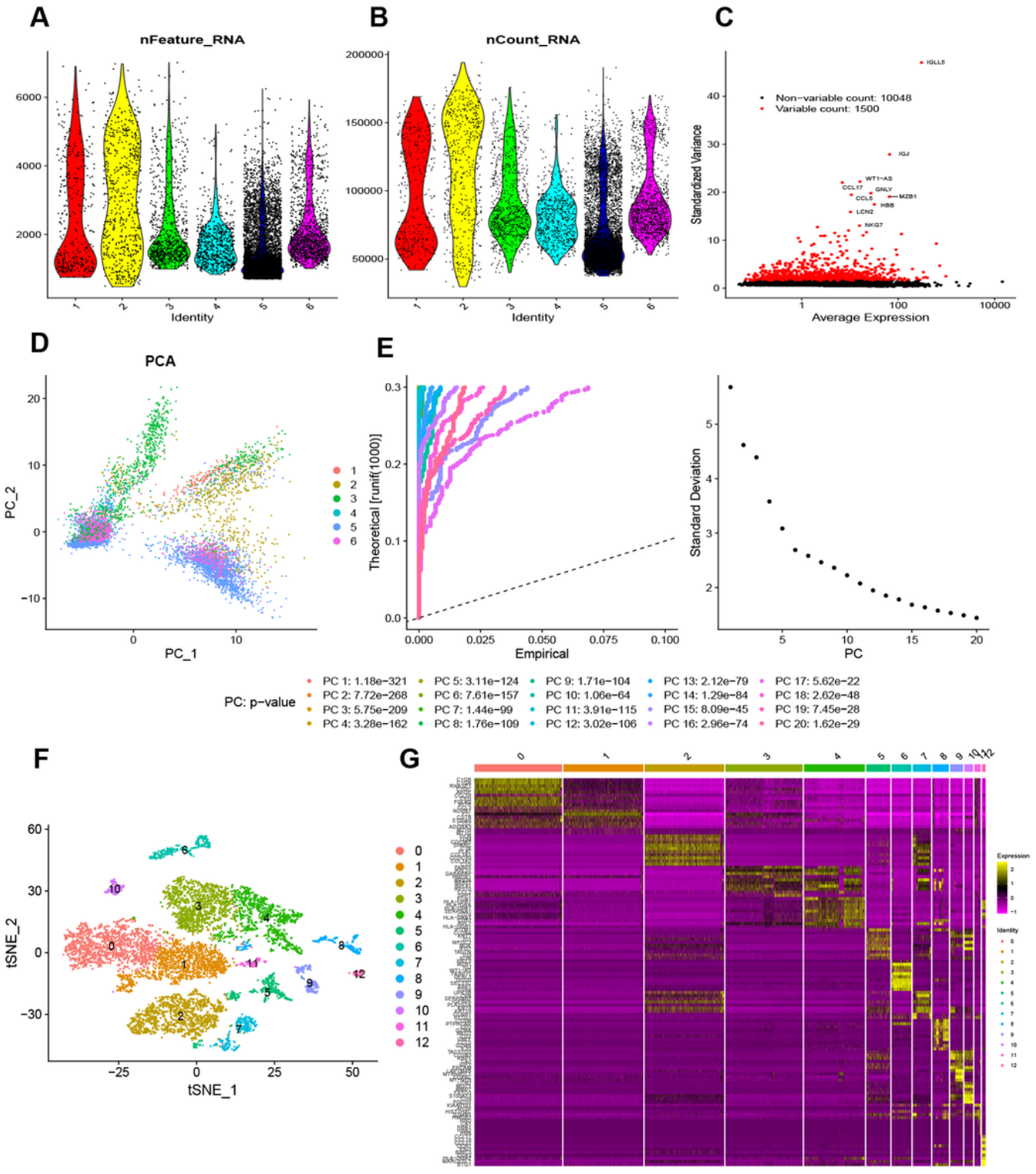

Figure 2

Heterogeneity in OV patients based on single-cell RNA-seq data. (A and B) 9609 cells from 6 OV patients were included in the analysis. (C) The variance diagram shows 10048 corresponding genes throughout all cells from OV. The top 10 hypervariable genes are shown in the plot. (D) PCA could not reveal clear separations of cells in OV. (E) PCA demonstrated the first 20 PCs with P value < 0.05. (F) Identification of 13 clusters by tSNE dimensionality reduction algorithm with the 20 PCs. (G) The heatmap showed the top

10 differential marker genes of each cell cluster. After removing the same marker genes among clusters, a total of 124 unique genes are listed.

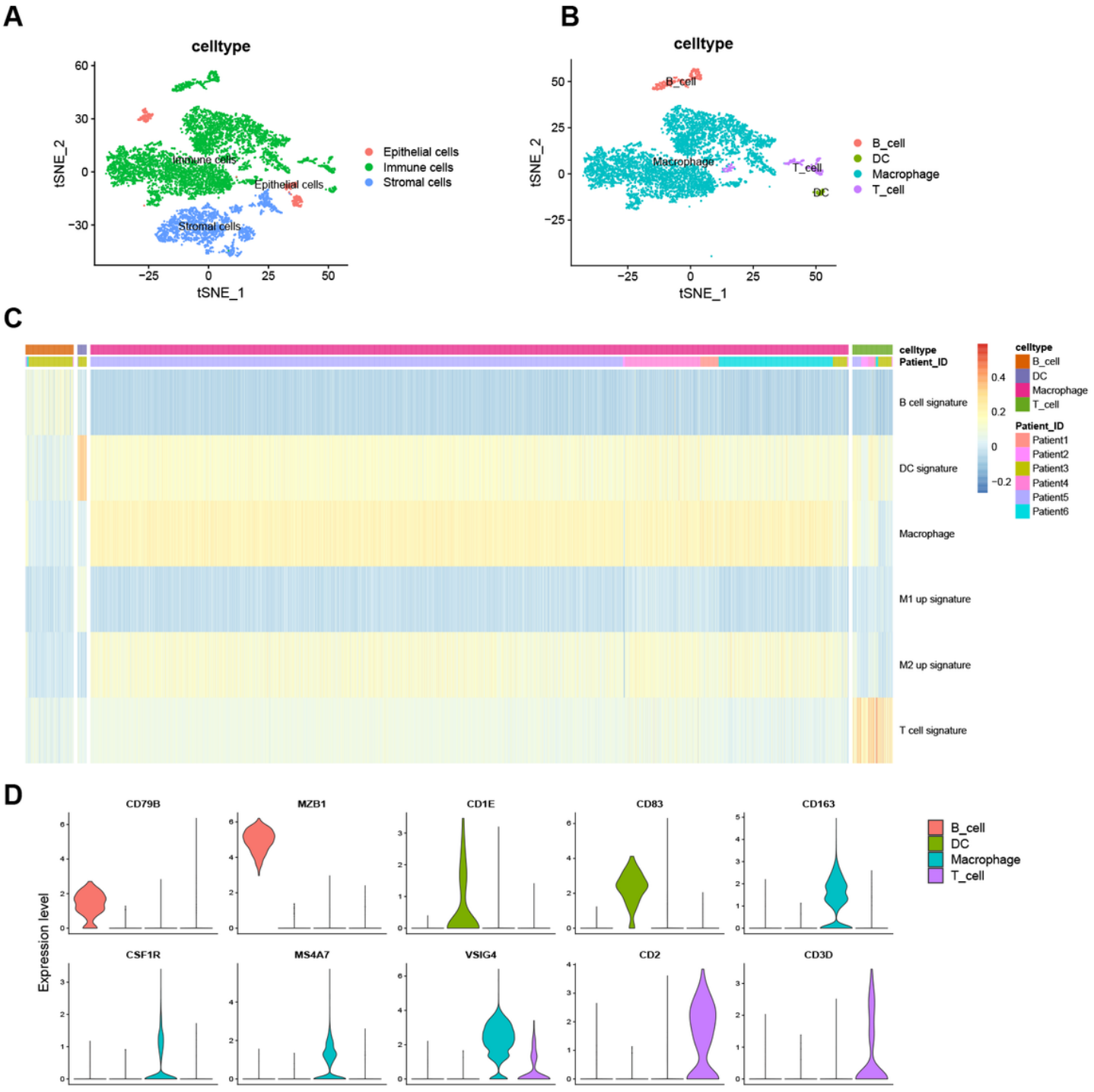

Figure 3

Clustering of immune cell populations and GSVA enrichment scores. (A) Cell-type visualized using tSNE dimensionality reduction reveals the clustering of tumor-stroma immune. (B) Tumor microenvironment immune cells were annotated into 4 subpopulations. (C) GSVA enrichment scores from gene set associated with B cells signature, DC signature, macrophages signature, M1 up signature, and M2 up

signature and T cells signature reveal a high proportion of M2 up signature occupying total macrophages in OV. (D) Violin plot indicates the important genes in immune cell subpopulations.

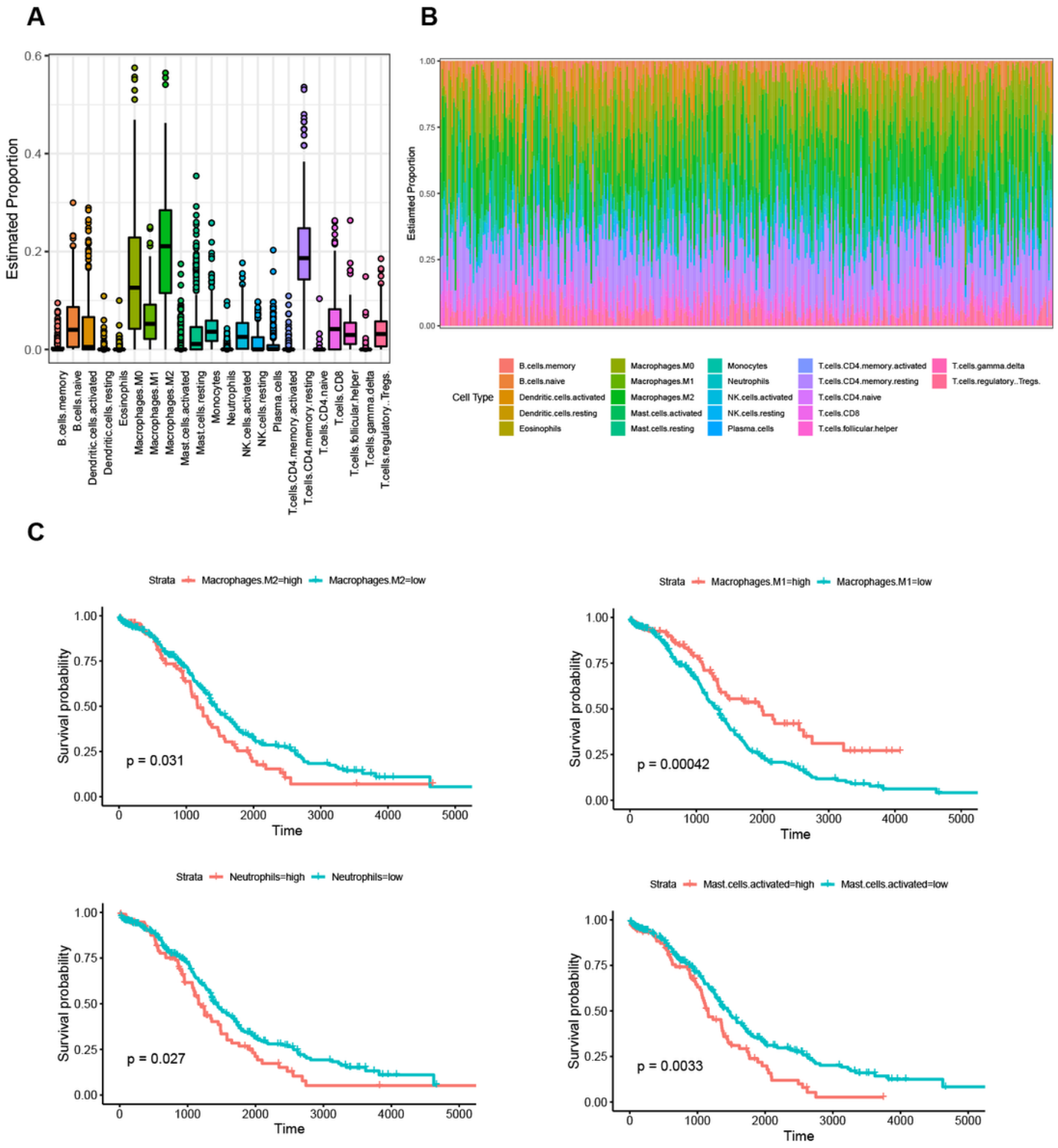

Figure 4

Tumor-infiltrating immune cell profile in OV samples and survival analysis. (A) Boxplot and Barplot(B) displayed the proportion of 22 kinds of TIC in OV tumor samples. (C) Kaplan-Meier overall survival analyses of macrophages M2, macrophages M1, mast cell activated, and neutrophils in TCGA-OV.

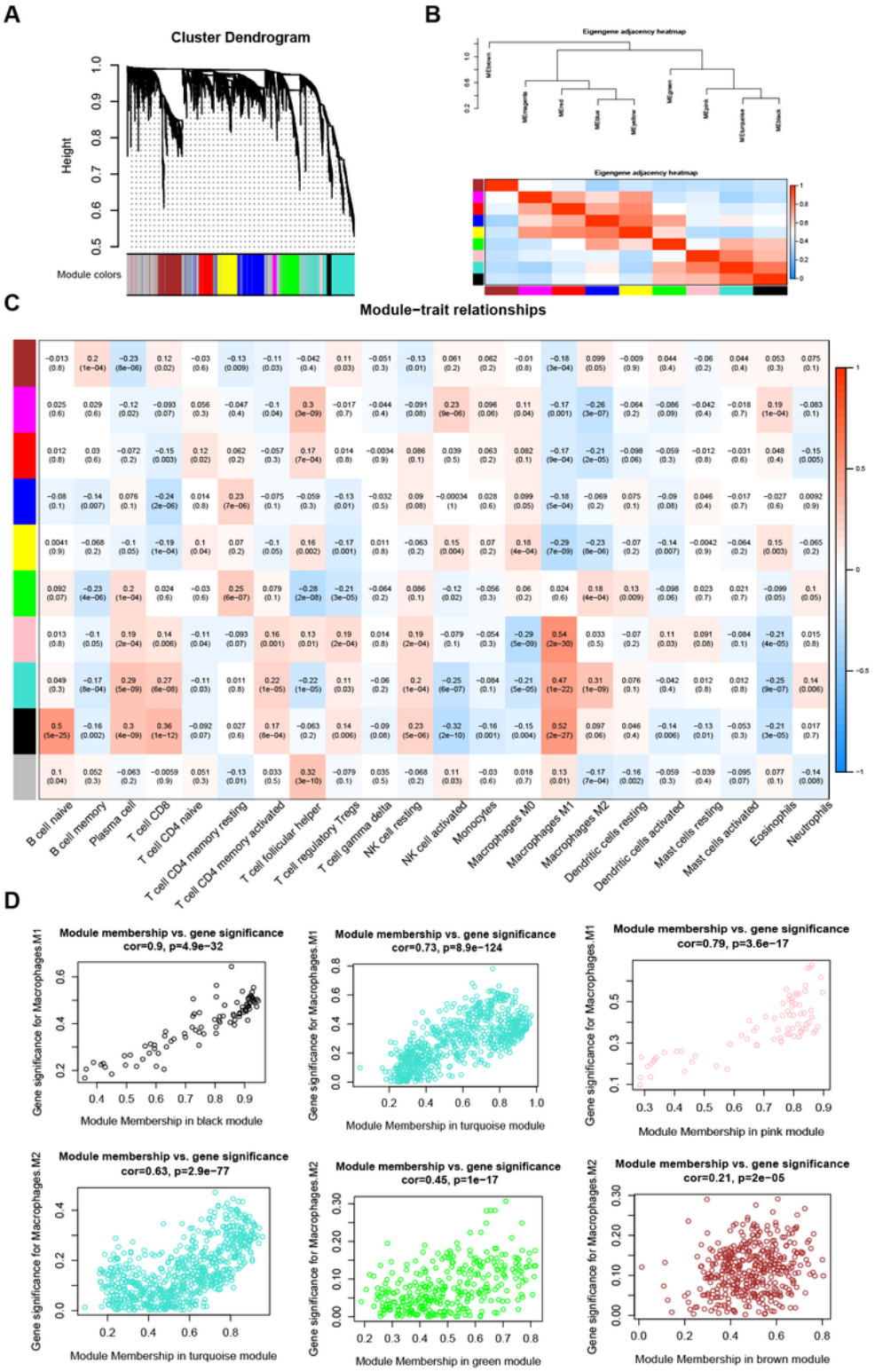

Figure 5

WGCNA analysis of co-expression modules. Construction of co-expression modules by weighted gene co-expression network analysis (WGCNA) package. (A) Dendrogram of the gene modules based on dynamic hybrid cutting, a total of 10 modules were constructed. (B) Heatmap and hierarchical clustering of the adjacencies in the hub gene network (C) Heatmap of the correlation between module eigengenes and the

proportion of tumor-infiltrating immune cells. (D) Scatter plot of macrophage M1 and macrophage M2 module eigengenes in three modules.

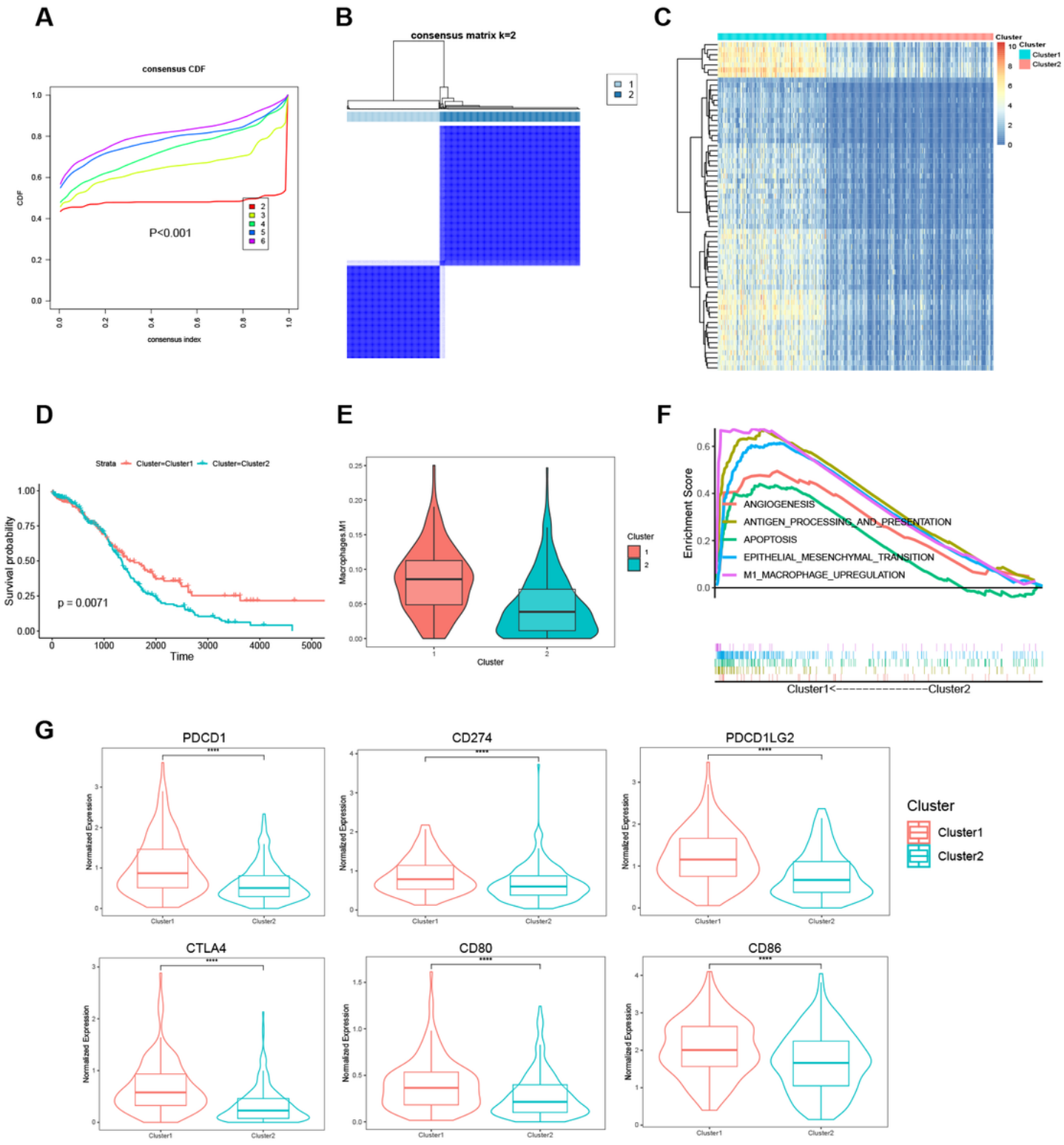

Figure 6

Identification of molecule subtype based on 219 TAM-related gene signature. (A) a CDF plot of the consensus score (k = 2-6). (B) Consensus clustering matrix for k=2. (C) Heatmap showed the differential expression genes between two clusters. (D) Kaplan-Meier analysis demonstrated that OV patients within

cluster 1 exhibited favorable OS. (E) Violin plots showed that TAM abundance was differentially distributed in identified subgroups (F) Upregulated hallmarks in the GSEA. (G) The expression of 6 immune checkpoints between two molecule subtypes.

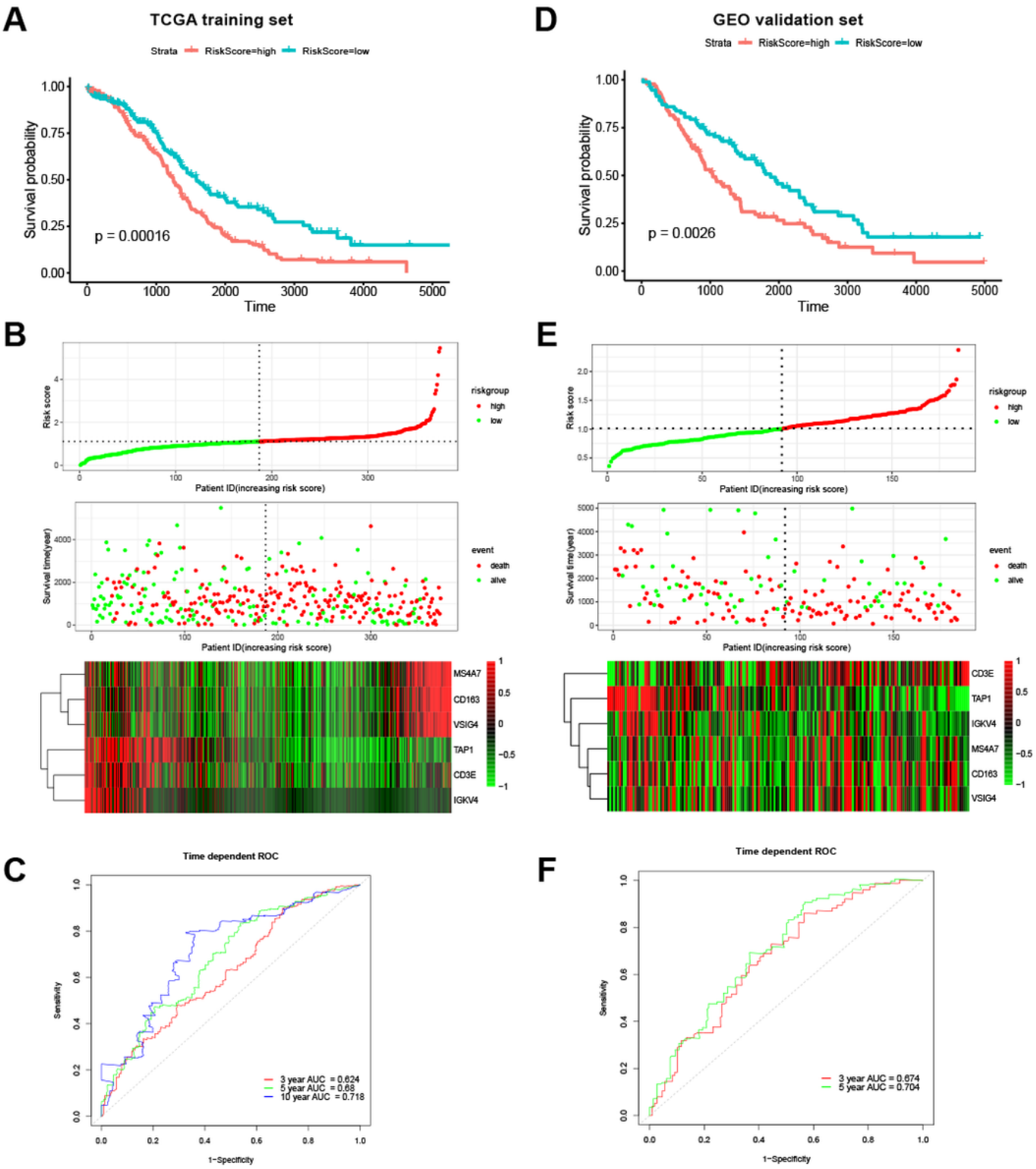

Figure 7

Prognostic analysis of the 6 gene signature risk score model in OV patients. Kaplan-Meier survival analysis was used to evaluate the OS of the high-risk and low-risk group in the TCGA training set (A) and

GEO validation set (D). Risk score analysis of the 6 gene signatures in the TCGA (B) and GEO (E) set, the dotted line represented the median risk score and divided the patients into low- and high-risk groups. Upper panel: The curve of risk score. Middle panel: Survival status and time of the patient. Bottom panel: Heatmaps of the expression levels of the 6 gene signature in the OV samples. Time-dependent ROC curve analysis was executed to estimate the prognostic performance of the 6 gene signature for predicting the 3-, and 5-year OS rates in the TCGA (C) and GEO sets (F).

Supplementary Files

This is a list of supplementary files associated with this preprint. Click to download.

- Supplementtable1.docx
- Supplementtable2.docx
- Supplementtable3.docx
- SupplemetFigure1.pdf
- SupplemetFigure2.pdf
- SupplemetFigure3.pdf
- Supplementfigure4.pdf